# Accepted Manuscript


A high-resolution HPLC-QqTOF platform using parallel reaction monitoring for in-depth lipid discovery and rapid profiling

Dingyi Yu, Thusitha W.T. Rupasinghe, Berin A. Boughton, Siria H.A. Natera, Camilla B. Hill, Pablo Tarazona, Ivo Feussner, Ute Roessner

PII: S0003-2670(18)30511-7

DOI: 10.1016/j.aca.2018.03.062

Reference: ACA 235889

To appear in: *Analytica Chimica Acta*

Received Date: 20 February 2018

Revised Date: 28 March 2018

Accepted Date: 30 March 2018

Please cite this article as: D. Yu, T.W.T. Rupasinghe, B.A. Boughton, S.H.A. Natera, C.B. Hill, P. Tarazona, I. Feussner, U. Roessner, A high-resolution HPLC-QqTOF platform using parallel reaction monitoring for in-depth lipid discovery and rapid profiling, *Analytica Chimica Acta* (2018), doi: 10.1016/j.aca.2018.03.062.

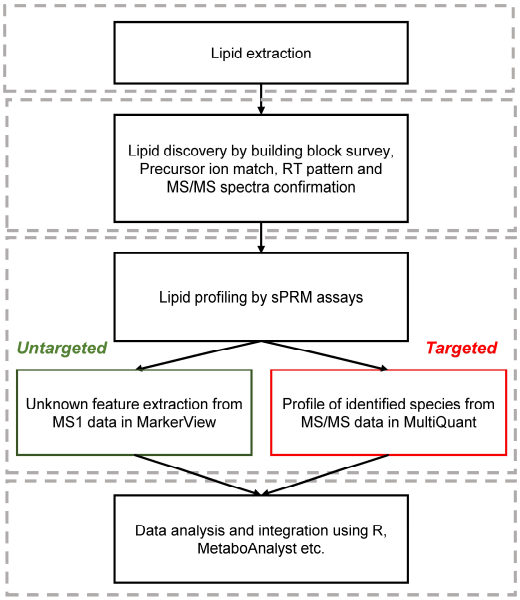


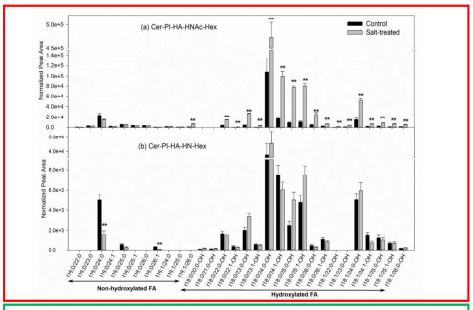


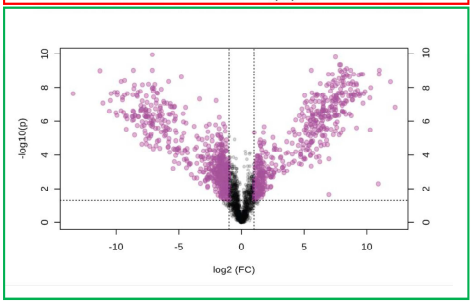

# A high-resolution HPLC-QqTOF platform using parallel reaction monitoring for in-depth lipid discovery and rapid profiling

**Dingyi Yu[1], Thusitha W.T. Rupasinghe[1, 2, *], Berin A. Boughton[1, 2], Siria H.A. Natera[1, 2], Camilla B. Hill[1,3], Pablo Tarazona[4,5], Ivo Feussner[4,6], Ute Roessner[1, 2]**

[1]School of BioSciences, University of Melbourne, Parkville, VIC, Australia, 3010

[2]Metabolomics Australia, School of BioSciences, University of Melbourne, Parkville, VIC, Australia, 3010

[3]Western Barley Genetics Alliance, Western Australian State Agricultural Biotechnology Centre, School of Veterinary and Life Sciences, Murdoch University, Perth, WA, Australia

[4]University of Goettingen, Albrecht-von-Haller-Institute for Plant Sciences, Department of Plant Biochemistry, Goettingen, Germany

[5]University of Goettingen, Albrecht-von-Haller-Institute for Plant Sciences, Goettingen Metabolomics and Lipidomics Platform, Goettingen, Germany

[6]University of Goettingen, Goettingen Center for Molecular Biosciences (GZMB), Department of Plant Biochemistry, Goettingen, Germany

Correspondence: Thusitha W.T. Rupasinghe

Address: School of BioSciences, The University of Melbourne, Parkville, VIC 3010, Australia

Tel: +61-3-8344-4806

E-mail: tru@unimelb.edu.au

**Abstract**

Here, we developed a robust lipidomics workflow merging both targeted and untargeted approaches on a single liquid chromatography coupled to quadrupole-time of flight (LC-QqTOF) mass spectrometry platform with parallel reaction monitoring (PRM). PRM assays integrate both untargeted profiling from MS1 scans and targeted profiling obtained from MS/MS data. This workflow enabled the discovery of more than 2300 unidentified features and identification of more than 600 lipid species from 23 lipid classes at the level of fatty acid/long chain base/sterol composition in a barley root extracts. We detected the presence of 142 glycosyl inositol phosphorylceramides (GIPC) with HN(Ac)-HA as the core structure of the polar head, 12 cardiolipins and 17 glucuronosyl diacylglycerols (GlcADG) which have been rarely reported previously for cereal crops. Using a scheduled algorithm with up to 100 precursors multiplexed per duty cycle, the PRM assay was able to achieve a rapid profiling of 291 species based on MS/MS data by a single injection. We used this novel approach to demonstrate the applicability and efficiency of the workflow to study salt stress induced changes in the barley root lipidome. Results show that 221 targeted lipids and 888 unknown features were found to have changed significantly in response to salt stress. This combined targeted and untargeted single workflow approach provides novel applications of lipidomics addressing biological questions.

**Keywords:** Lipidomics; Mass spectrometry; Parallel reaction monitoring; Salt stress.

**Abbreviations:** MRM: multiple reaction monitoring; QqQ: triple quadrupole; QTRAP: quadrupole linear-ion trap; UHPLC: ultra-high performance liquid chromatography; QqTOF: quadrupole time-of-flight mass spectrometry; sPRM/uPRM: scheduled/unscheduled parallel reaction monitoring; RT: retention time; MRM-hr: high-resolution MRM; PBQC: pooled biological quality control; ASG: acylated sterol glucoside; CDS: calibrant delivery system; CE: collision energy; Cer: ceramide; CL: cardiolipin; DAG: diacylglycerol; DGDG: digalactosyl diacylglycerol; DGMG: digalactosyl monoacylglycerol; DP: declustering potential; EICC: extracted ion count chromatogram; FC: fold change; FDR: false discovery

rate; G1/2/3: Gradient 1/2/3; GIPC: glycosyl inositol phosphorylceramide; GL: glycerolipid; GlcADG: glucuronosyl diacylglycerol; GlcCer: glucosyl ceramide; GP: glycerolphospholipid; HexCer: monohexosyl ceramide; HA: hexuronic acid; Hex: hexosyl; HN: N-acetylhexosamine; HNAc: hexosamine; HRMS: high-resolution mass spectrometer; IPC: inositol phosphoryl ceramide; ISVF: ion spray voltage floating; LCB: long chain base; MGDG: monogalactosyl diacylglycerol; MGMG: monogalactosyl monoacylglycerol; Neg: negative ion mode; OAc: acetate; PC: phosphatidylcholine; PCA: principal component analysis; PE: phosphatidylethanolamine; PG: phosphatidylglycerol; PI: phosphatidylinositol; Pos: positive ion mode; PS: phosphatidylserine; SG: sterol glycoside; SP: sphingolipid; SQDG: sulfoquinovosyl diacylglycerol; SQMG: sulfoquinovosyl monoacylglycerol; ST: sterol derivative; THF: tetrahydrofuran; VLCFA: very long chain fatty acid.

## 1. Introduction

Lipidomics is an emerging technology and a branch of metabolomics which aims at the global characterisation and quantification of lipids within biological matrices including biofluids, cells, whole organs and tissues [1]. In the past 15 years, the field of lipidomics has been largely driven by advances in modern analytical techniques, especially mass spectrometry. Targeted and untargeted lipidomics are the two major approaches used in mass spectrometry-based lipidomics. Untargeted lipidomics involves a non-biased screening of all the potential lipids in a sample but is often limited in sensitivity and selectivity. By contrast, targeted lipidomics is both sensitive and accurate for lipid analysis, but focuses only on expected (or known) lipid species while unknown lipid species are not detected [2]. To reveal the suite of differences between lipids and other metabolites, a combination of different platforms and techniques is often employed [3, 4]. Traditionally, a targeted strategy is achieved by employing multiple reaction monitoring (MRM) on a triple quadrupole (QqQ) or quadrupole linear-ion trap (QTRAP) coupled to high performance liquid chromatography (HPLC) or ultra-high performance liquid chromatography (UHPLC) [2]. Untargeted lipidomics techniques employ high-resolution mass spectrometers (HRMS) including TOF, FT-ICR or Orbitrap platforms with high resolution and high mass accuracy to resolve isobaric lipid species which have the same nominal mass but different exact masses [2, 4]. However, one limiting factor of using multiple platforms is the high economic cost of maintaining and operating several instruments, as well as the computationally more demanding integration of datasets from different platforms. In addition, different instrumental conditions and parameters used for ionization and fragmentation during MS/MS can lead to severe difficulties when integrating targeted and untargeted data.

Parallel reaction monitoring (PRM), also referred to as high-resolution multiple reaction monitoring (MRM-hr), is an example of a recently developed acquisition strategy to integrate targeted and untargeted data by combining HPLC with quadrupole-equipped HRMS [5]. In a PRM assay, a duty circle in the MS is often initiated with a MS1 survey scan followed by a series of targeted MS/MS experiments. The MS1 survey collects untargeted high-resolution mass spectra enabling profiling of all precursors across a large

*m/z* range (approximately 50 − 2000 *m/z*). A MS/MS experiment in PRM mode isolates a preset precursor ion in the quadrupole and detects all product ions generated from collision-induced dissociation (CID) on the HRMS [6]. PRM has been shown to successfully enable quantitative studies in both proteomics and metabolomics applications [5, 7-9]. Very recently, Zhou et al. used a SCIEX 4600 TripleTOF™ system to monitor 222 lipid species from 15 lipid classes in human serum in PRM mode [10]. Compared with traditional MRM on QqQ instruments, PRM offers more accurate *m/z* and narrower peak width of ions in MS spectra. The high resolution and mass accuracy of the resulting MS/MS spectra enables more precise identification of product ions of the corresponding precursor ion. Moreover, with full MS/MS spectra obtained in PRM mode, selection of fragment ions for targeted profiling can be determined post data acquisition. Intensities of multiple fragment ions can also be summed to achieve better sensitivity [5].

One of the weaknesses of targeted analysis by MS/MS experiments in PRM is the low scan rate which limits the capability of MS/MS experiments when performed on a large-scale [8, 11]. Recent technological advances have included increased scan and data acquisition rates on quadrupole time-of-flight mass spectrometry (QqTOF) instruments to allow for multiplexing large-scale numbers of precursors [11, 12]. The latest SCIEX TripleTOF™ 6600 QqTOF can deliver up to 100 MS/MS experiments per duty cycle with high sensitivity and resolution achieving considerable throughput gains in targeted monitoring [11]. Furthermore, implementing retention time (RT) scheduling significantly increases the capacity for targeting compounds during a whole LC chromatogram [8, 13]. In scheduled acquisition, each compound is monitored for a short period of time in a specific time window around the expected RT. This expands the total number of overall precursors that can be monitored in a single LC-MS run without sacrificing accumulation or duty cycle time.

In previous PRM applications, the MS1 survey scan was often used only as a complementary profiling strategy [9]. To exploit the full potential of MS1 scans, a greater number of mass features with specific RTs, *m/z* and intensities can be extracted and used to produce a global lipid profile of the whole sample extract.

Lipids are important signaling messengers and membrane structural regulators that play roles in many plant responses, including those to abiotic stresses such as salinity and drought [14-16]. Barley is one of the most salt-tolerant cereal crops and has been used as a model plant to study salt stress in recent years [17]. Natera et al. studied salt-induced lipid compositional changes of two barley varieties differing in their ability to tolerate salinity [18]. A total of 708 mass features were extracted from untargeted HPLC-ESI-QqTOF analysis and 64 lipid species quantified by HPLC-ESI-QqQ analysis were compared. A range of alterations induced by salt stress were observed particularly for glycerophospholipids.

In our study, we demonstrate the applicability of parallel analysis of untargeted and targeted lipidomics by taking advantage of both untargeted profiling by MS1 and targeted analysis by MS/MS experiments. This novel approach enables the discovery of a large number of unidentified lipid species, while simultaneously identifying fatty acid composition and the head group of most of the lipid species. In addition, this robust lipidomics platform using sPRM mode on a HPLC-ESI-QqTOF was established to achieve comprehensive lipidome investigation of barley root extracts and to apply the platform to the study of plant salinity stress.

## 2. Materials and methods

### *2.1 Lipid nomenclature and abbreviations*

Lipid nomenclature used across the manuscript follows the "Comprehensive Classification System for Lipids" presented by the International Lipid Classification and Nomenclature Committee (ILCNC) [19]. The nomenclature can be viewed online on the LIPID MAPS website (http://www.lipidmaps.org/data/classification/LM_classification_exp.php). However, structural information gained from mass spectrometry is usually insufficient to cover the precise structural information of LIPID MAPS nomenclature, requiring the use of an additional notation for simplified mass spectrometry-based information. In this paper, we adopted the simplified notation developed by Liebisch et al. [20]. For example, the nomenclature PC(16:0/18:2) designates a phosphatidylcholine with fatty acyl chains of length 16:0 and 18:2 found on the *sn*-1 and *sn*-2 position of the glycerol backbone respectively. The nomenclature PC(16:0_18:2) indicates a PC species with two fatty acyl chains, 16:0 and 18:2, but that the exact *sn*-position of the esterified FA is unknown. The nomenclature PC(34:2) indicates a PC species with a fatty acyl sum composition of 34 carbons containing 2 unsaturated double bonds, with fatty acyl identity and position not yet resolved.

Abbreviations used for lipid or related chemicals were as follows: ASG: acylated sterol glucoside; Cer: ceramide; CL: cardiolipin; DAG: diacylglycerol; DGDG: digalactosyl diacylglycerol; DGMG: digalactosyl monoacylglycerol; GIPC: glycosyl inositol phosphorylceramide; GL: glycerolipid; GlcADG: glucuronosyl diacylglycerol; GlcCer: glucosyl ceramide; GP: glycerolphospholipid; HexCer: monohexosyl ceramide; Hex: hexosyl; HN: N-acetylhexosamine; HNAc: hexosamine; HA: hexuronic acid; IPC: inositol phosphoryl ceramide; LCB: long chain base; MGDG: monogalactosyl diacylglycerol; MGMG: monogalactosyl monoacylglycerol; PC: phosphatidylcholine; PE: phosphatidylethanolamine; PG: phosphatidylglycerol; PI: phosphatidylinositol; PS: phosphatidylserine; SG: sterol glycoside; SP: sphingolipid; SQDG: sulfoquinovosyl diacylglycerol; SQMG: sulfoquinovosyl monoacylglycerol; ST: sterol derivative.

152 *2.2 Chemicals and lipid standards*

153 Methanol (LC-MS grade) was purchased from Fisher Scientific (Scoresby, VIC, Australia); Hexane (LC
154 grade) was from Honeywell (Taren Point, NSW, Australia); 2-propanol (LC-MS grade) was from RCI
155 Labscan (Bangkok, Thailand). Deionized water was produced by a Millipore Milli-Q system (Billerica,
156 MA, USA). Standards of PC(13:0/13:0), PE(12:0/12:0), PS(12:0/12:0), PI(18:0/20:4), PG(12:0/12:0),
157 LysoPC(13:0), LysoPE(13:0), LysoPI(13:0), LysoPG(13:0), Cer(d18:1/12:0), GlcCer(d18:1/12:0),
158 CL(14:1/14:1/14:1/14:1) [CL(T14:1)] and DAG(18:0/20:4) were purchased from Avanti Polar Lipids
159 (Alabaster, Alabama, US). A mixture of 13 lipid standards was prepared as a stock solution at a
160 concentration of 1 mM in methanol/chloroform 1:1 (v/v) and stored at −20 $^{o}$C. All other chemicals were
161 purchased from Sigma-Aldrich (Castle Hill, NSW, Australia).
162
163 *2.3 Sample preparation and lipid extraction*
164 Seeds of barley (*Hordeum vulgare* L.) genotype *Mundah* were provided by the University of Adelaide
165 (SA, Australia). Barley was grown in hydroponics for 5 weeks as described previously [21]. Salt
166 treatment was implemented with a concentration of 250 mM NaCl in hydroponics solution for three
167 weeks. Roots were quickly separated from shoots with sterilised scissors, gently washed with distilled
168 water to remove remaining hydroponics solution, frozen in liquid nitrogen and stored at −80 $^{o}$C until
169 extraction.
170 To extract lipids, frozen roots were homogenized into a fine powder using liquid nitrogen and a mortar
171 and pestle. Lipids were extracted according to the procedure previously described by Grillitsch et al [22].
172 Homogenized barley root powder (250 − 300 mg) was quickly delivered into a monophasic mixture of 2-
173 propanol/hexane/water 60:26:14 (v/v/v, 6 mL) and incubated at 60 °C for 30 min in an Eppendorf
174 Thermomixer Comfort (Hamburg, Germany) at 500 rpm. Samples were vortexed for 10 s and sonicated
175 for 1 min every 10 min during incubation. The extract was centrifuged at 2,000 g for 20 min at room
176 temperature. The supernatant was transferred to a new tube, evaporated to dryness under a stream of
177 nitrogen, then re-constituted in 500 µL of 2-propanol/methanol/water 4:4:1 (v/v/v) and stored at −20 °C.

A total of four biological replicates were prepared. In order to compensate for variations in sample preparation and ionization efficiency, a total of 10 μL of internal standard mixture, consisting of 100 μM of PE(12:0/12:0) and Cer(d18:1/12:0), was spiked into each replicate prior to extraction. A pooled biological quality control (PBQC) sample was produced by collecting 150 μL from each replicate as described previously [23].

To evaluate profiling performance of PRM assays, extra barley root extracts were prepared and spiked with the mixture of 13 lipid standards. Six concentrations (0.01, 0.05, 0.20, 1, 5, 20 μM) of each standard lipid species were measured in triplicate in PRM mode.

*2.4 HPLC-ESI-QqTOF conditions*

The barley root extracts and lipid standards were analysed using an Agilent 1290 HPLC system (Santa Clara, CA, USA) coupled to a SCIEX TripleTOF$^{TM}$ 6600 QqTOF mass spectrometer (Framingham, Massachusetts, USA). The 6600 TripleTOF$^{TM}$ was equipped with a Turbo V$^{TM}$ dual-ion source (ESI and APCI) and an automated calibrant delivery system (CDS).

Separation of most lipid species was carried out using an Agilent Poroshell EC-C18 (100 mm × 2.1 mm, 2.7 μm, Col A) at a flow rate of 0.40 mL/min at 50 $^{o}$C with an exception for glycosyl inositol phosphorylceramides (GIPCs) which were independently analysed using an Agilent ZORBAX Eclipse XDB C18 (100 mm × 2.1 mm, 1.8 μm, Col B) at a flow rate of 0.20 mL/min at 50 $^{o}$C. Three linear gradients based on two mobile phases: mobile phase A, methanol/20 mM ammonium acetate 3:7 (v/v); and mobile phase B, 2-propanol/methanol/20 mM ammonium acetate 6:3:1 (v/v/v) were applied for different lipid classes (Figure 1). Gradient 1 (G1) and 2 (G2) were performed at a flow rate of 0.4 mL/min with starting conditions of 65% and 80% B for 2 min, respectively. The subsequent conditions of G1 and G2 were then the same: linear increase to 100% B for 8 min, followed by 100% B for 6 min and then re-equilibration to starting conditions in 2 min. Gradient 3 (G3), specifically for GIPCs on Col B, had a flow rate 0.20 mL/min starting with 80% B for 2 min, followed by a linear increase to 100% for 8 min, 100% B held for 6 min and then re-equilibration to starting conditions in 2 min. Gradients and adducts of the

targeted analytes from the 23 lipid classes used in all PRM assays are listed in Table 1. Collision energies (CEs) optimized for each lipid class were as follows: −45 V for PC, PE, PG, MGDG, DGDG, PS and all Lyso-species; −65 V for PI, SQDG, GlcADG and CL; +40 V for Cer, HexCer, ASG, SG and DAG; +65 V with 10 V collision energy spread (CES) for GIPC. ESI parameters were optimized and preset for all measurements as follows: Source temperature, 450 °C; Curtain gas, 45 psi; Gas 1, 45 psi; Gas 2, 45 psi; Declustering potential (DP): +100 V in positive ion mode, −200 V in negative ion mode; Ion spray voltage floating (ISVF) was set to −4,500 V in negative ion mode and +5,500 V in positive ion mode. Instrument was calibrated automatically via the CDS delivering APCI calibration solution (Foster City, CA, USA) every 10 samples. CDS injected either positive or negative APCI calibration solution depending on the polarity of ESI and calibrated the mass accuracy of the 6600 TripleTOF™ system in both ionization modes including TOF-MS and high-sensitivity MS/MS. With calibration, the mass resolution for precursor ions in MS1 spectra was ~35,000, while the resolution for the resulting fragments in high sensitivity MS/MS scans (PRM transitions) was ~20,000. Actual mass accuracy was below 5ppm in MS1 spectra and 10 ppm in MS/MS spectra.

sPRM assays with a detection window of 120 s were composed of a MS1 scan (250 ms, scan range: 100 – 2000 Da) followed by different number of targeted MS/MS scans (25 ms, scan range: 100 – 1600 Da) resulting in an instrument duty cycle time of between 1 and 2 s. These settings allowed a minimum of 10 data points to be collected across each chromatographic peak. Parameters of targeted precursor information on PRM assays including *m/z*, predicted RTs and RT window width were entered to 6600 TripleTOF™ Analyst acquisition software (Version 2.2) via Skyline software as described by Schilling et al. [5].

*2.5 Data processing*

*2.5.1 Mass feature extraction from MS1 data*

MarkerView software (Version 1.2, SCIEX, Framingham, Massachusetts, USA) was used to extract mass features from both positive (G2) and negative (G1) ion mode MS1 data. Mass features were extracted for

ions with a *m/z* range of 100 to 1,600 eluting between 0.5 and 16 min. Noise threshold was set at 300. RT and *m/z* alignment of the mass features were performed with tolerances of 5% and 0.01 Da, respectively. Intensities were normalised by manual scale factor, which is calculated from an internal standard intensity and sample weight. Only features that were detected in at least three samples of each group were extracted. Only features which contained an isotopic partner were selected for further data analysis. RTs were aligned by internal standards.

*2.5.2 Peak picking for lipid profiling based on MS/MS data*

Lipid profiling using MS/MS data in PRM assays was based on the peak area of extracted ion count chromatogram (EICC) for one or multiple fragment ions in MultiQuant (Version 3.0.2). For glycerol-based monoacyl and diacyl lipids as well as CLs performed in negative ion mode, peak area of all negative charged FA fragments were summed; while for DAGs detected in positive ion mode, total peak area of all fragments resulting from neutral loss of a FA chain was used. For SPs, the sum of peak area of positively charged long chain base (LCB) and its dehydrates from up to three dehydration processes were used for profiling HexCer and Cer species. For STs, the dehydrated sterol backbone was the only fragment chosen. Peak picking for fragment ions was finally set to 100 ppm width. Integration settings were as follows: Noise percentage = 40%; Gaussian smooth width = 2 points. Peak areas were normalized based on the intensity of internal standards and sample weight.

*2.5.3 Statistical analysis*

For both targeted and untargeted analysis, peak areas of compounds/features in each sample (control and salt-treated) were acquired and normalised to the value equivalent to 250 mg fresh sample weight. Student's *t*-tests were conducted on each compound/feature to evaluate for significance (*p*-value) between two groups. Adjusted *p*-values were obtained with Benjamini-Hochberg false discovery rate (FDR) correction. The heatmap was plotted using the heatmap package (Version 1.0.8) in R using Euclidean

255 distances and the Ward's algorithm. Principal component analysis (PCA) plots with the pareto scaling as
256 well as volcano plot were generated in MetaboAnalyst (Version 3.0).
257

## 3. Results and discussion

### *3.1 Optimization of chromatography conditions*

The lipid separation was carried out on reversed phase columns with mobile phases modified from a previously developed lipidomics platform by Tarazona et al. [3]. To improve compatibility of the mobile phases with our instruments, THF was replaced by 2-propanol, which has a similar polarity index (3.9) as THF (4.0). A significant disadvantage of 2-propanol as a mobile solvent is the relatively higher viscosity (2.4 cP at 20°C; THF: 0.55 cP at 20°C) which can generate high back pressure especially on HPLC columns containing particles of small size. At a flow rate of 0.40 mL/min with 100% mobile phase A (2-propanol), the back pressure can reach up to 1,100 bar when using an Agilent ZORBAX Eclipse XDB C18 (100 mm × 2.1 mm, 1.8 μm, Column B). This high back pressure was overcome by using a low flow rate (0.20 mL/min) or using a core-shell column (Agilent Poroshell 120 series) with larger particle size (2.7 μm) to achieve similar performance  Three gradients, two for positive and one for negative ion mode, were then applied and optimized. For profiling most GP and GLs, charged FA fragments were chosen. There is the possibility of interference arising from the M+2 isotopologue during identification, so to avoid this scenario chromatographic conditions were optimized to separate lipid species (Figure 2b). In SPs, positively charged LCBs and their dehydrated fragments were used for profiling. SP species which only have a double bond difference on the LCB were also optimized to prevent isotopic interference.

### *3.2 Lipid identification from MS1 and MS/MS data*

#### *3.2.1 Overall strategies and workflow*

Identification of lipid species followed a combination of three filtering criteria described by David et al. [24]: (i) MS1 spectra featuring high mass resolution (~ 35,000) and accurate mass (< 5 ppm) for fast and straight-forward precursor ion search against a compiled list; (ii) RT behavior on a C18 column related to characteristics of molecular structure (double bond/total carbon number/hydroxyl group number in FA/LCB/sterol backbone etc.), which can significantly reduce false annotation caused by interference from isobaric/isomeric species, in-source fragments; and (iii) complete high-resolution MS/MS spectra

from MS/MS experiments in both ESI positive and negative ion modes that capture characteristic fragments enabling validation.

Methodologically, we first followed the approach of Tarazona et al. [3] to compile a target list based on building block survey information (see Supplementary data) and previously published literature [3, 25] (Figure 1). The compiled list contains over 3,000 possible lipid species from 23 lipid classes. Then, a concentrated PBQC sample was analysed using unscheduled PRM assays for MS1 and MS/MS spectra collection. Lipid identification was first done using MS1 data to search against the compiled list. With high resolution and mass accuracy of MS1 spectra, we employed a strict MS1 precursor match (< 5 ppm) combined with RT behavior restriction to identify lipid species. To further validate all lipid species detected using MS1 data, MS/MS spectra acquired from MS/MS experiments from both ESI positive and negative ion modes were compared with previous literature [25-27] or the publicly available databases, LIPID MAPS and LipidBlast [28].

Research by Tarazona et al. [3] utilised a platform combining HPLC-ESI-QqTOF and HPLC-NanoESI-QTRAP to investigate alterations of lipids from four categories — glycerolipids (GL), glycerophospholipid (GP), sphingolipid (SP), sterol derivatives (ST) in *Arabidopsis* under cold and drought stress. A record number of 393 species in 23 lipid classes were identified and then quantified in MRM mode on a HPLC-NanoESI-QTRAP. When compared to their target list, a more extensive lipid coverage was achieved in our experiments in above four categories with over 600 lipid species from 23 lipid classes, including 209 GPs, 190 GLs, 215 SPs and 20 STs analysed. Table 2 summarizes the number of lipid species detected in each lipid class within the four categories. Detailed information of all identified individual lipid species, including lipid class, compound name, precursor *m/z*, RTs and qualitative fragments in MS/MS spectra can be found in the Supplementary data (Table S1).

*3.2.2 Glycerolipids and glycerophospholipids*

Neutral GP species such as DAGs exhibited much higher ionization efficiency in positive ion mode as ammonium adducts than as acetate anion adducts in negative ion mode in our system. GP and polar GL

310 species (PC, PE, PG, PI, PS, MGDG, DGDG, SQDG, GlcADG, CL, lyso-species) could be ionized in
311 either ion mode in the presence of $NH_4OAc$. In negative ion mode, fragmentation of GP and polar GL
312 species yielded rich characteristic ions corresponding to the fatty-acyl group esterified at the *sn*-1 or/and
313 *sn*-2 positions; while in positive ion mode there were abundant fragments from either charged or neutral
314 loss of the polar head instead of fragments from FAs. RTs of GPs and GLs in reversed phase
315 chromatography have an increasing correlation in relation to the total number of carbon atoms and a
316 competing decreasing correlation as the total number of unsaturations increases with respect to retention
317 time of the least unsaturated precursor.
318 Lyso-GP and lyso-GLs are lower mass lipids containing only one fatty acyl chain. Over 80 lyso-GPs and
319 lyso-GLs with varying acyl chain lengths from C14 to C26 were identified by comparison to the MS1
320 database (search using mass error < 5 ppm) coupled to MS/MS spectra identifying the FAs.
321 Diacyl-GP GLs observed by MS1 scan could only be represented as the sum of fatty acyl chains, as from
322 MS1 data alone it is not possible to determine the fatty acyl distribution on the glycerol backbone. Using
323 MS/MS data, a substantial number of constitutional isomers with the same sum fatty acyl composition but
324 differing in FA chains could be resolved (Figure 2b). Using MS/MS scans in negative ion mode, the
325 transition of each precursor to specific charged FAs could differentiate the respective isomers, even when
326 they co-eluted. For example, using this methodology we were able to identify 43 PE species including 13
327 pairs of isomers, covering a total FA chain length from C30 to C44 (Figure 2a).
328 All detailed diacyl-GPs identified at level of FA composition are listed in supplementary data (Table S1).
329 Notably, a recently discovered novel plant GL class, GlcADG [29] , was found including a total of 17
330 species with summed FA chain length ranging from C32 to C36.
331 CLs were found containing only C16 and C18 fatty acyl chains, with at least two of the four fatty acyl
332 chains detected in CL species found to be C18, forming a total chain length from C68 to C72.
333

*3.2.3 Sphingolipids*

HexCer, Cer and GIPC species, all of which containing ceramide in the molecule structure can be detected as $[M+H]^+$ and $[M+Na]^+$ in positive ion mode or $[M-H]^-$ and $[M+OAc]^-$ in negative ion mode. Previous studies of the Cer class have shown increased sensitivity for the respective precursor ion in negative ion mode when compared to the corresponding precursor ion in positive ion mode [30]. However, MS/MS product ion spectra of $[M+H]^+$ precursors contained high resolution mass spectra and were easier to interpret and assign both fatty-acyl amide substituents and the LCB when compared to the deprotonated precursors.

Both isomeric and isobaric interferences were problematic when attempting to identify ceramide-containing plant SP species. With a resolving power of ~35,000 and < 5 ppm in MS1 spectra, differentiation of some isobaric SP species such as Cer(t18:0/23:0-OH) (*m/z* 668.6193, $ESI^+$) and Cer(t18:0/24:0) (*m/z* 668.6557, $ESI^+$) can be achieved. However, for near-isomeric and isomeric SP species, MS1 spectra alone is not enough to precisely annotate them. As an example, the isomers HexCer(t18:1/24:0-OH) and HexCer(t18:0/24:1-OH) were predicted as the *m/z* 844.687 in MS1 scan in positive ion mode but an EICC of *m/z* 844.687 showed three intense peaks at 8.44, 8.91 and 9.47 min respectively (Figure 3a). Further examination of the respective MS1 spectra indicated that the peaks at 9.47 and 8.91 min likely corresponds to the two isomers and that the peak at 8.44 min likely corresponds to an interference generated from the M+2 isotopologue of HexCer(t18:1/24:1-OH). Also, in-source dissociation raised another challenge to SP identification. Cer and HexCer cations could dehydrate under the source conditions used and a proportion of the hexose head-groups of HexCer and GIPC molecules were cleaved during the ionization process (Figure S2, Supplementary data). The in-source dissociation generated both intra-class interference in Cer, HexCer and GIPCs as well as inter-class interference. For example, the in-source hexose head cleavage of HexCer species generates an ion corresponding to a possible Cer, thereby producing interference when identifying Cer species. The in-source dehydration caused intra-classes interference between lipid species with a $H_2O$ difference in molecular structure such

as between SPs containing t18:1 and d18:2. It is hard to rule out possible head-group cleavage and/or dehydration and accurately identify sphingolipid species by examination of the MS1 spectra alone.

One key point of differentiation was the cluster of fragments related to the positively charged LCB found in MS/MS spectra. For example, SPs with a t18:0 LCB exhibited ions with *m/z* 318.301, 300.293, 282.280 and 264.270, resulting from the charged LCB and three dehydration processes on fragmentation; while a cluster of fragment ions *m/z* 316.287, 298.276, 280.266 and 262.256 indicated existence of t18:1 LCB (Figure 3a). RT patterns related to FAs, LCBs and polar head were another important factor in distinguishing between interferences. For SP species in the same class, containing same FA but different LCBs, RT values based on LCBs were t18:1 < d18:2 < t18:0 < d18:1 (Figure 3b). RT values also reduced as more sugar units were attached to the head-group on the ceramide backbone. For example, specific Cer species generally elute 0.8 – 1 min later than the corresponding HexCer species (Figure 3b).

As a result, 26 Cer species and 47 HexCer species were identified. Ceramide was detected with only t18:0 (n = 17) and t18:1 (n = 9) LCBs; while HexCer species were predominantly d18:2 and t18:1 (n = 15) species, with d18:1 and t18:0 as minor components. C24 FAs are the main fatty acids in Cer with the three most intensive Cer species being Cer(t18:0/24:1-OH), Cer(t18:0/24:0-OH) and Cer(t18:1/24:1-OH). Contrastingly in HexCer, HexCer(t18:0/16:0-OH) was likely to be the most abundant species.

The structure of GIPCs consists of a ceramide moiety and a polar head containing sugars linked to a phosphorylated inositol. Combinations of different numbers and types of sugar, and connectivity in the head group can form diverse structures of GIPCs across different plant species [31]. To our knowledge, no reports exist that describe either qualitative or quantitative analyses of GIPCs in barley.

In our experiment, we identified GIPCs in barley roots and characterised the polar head using product ion surveys on a set of putative precursors from different forms [32]. The Hex-HA-IPCs found in *Arabidopsis* were not detected in barley roots using either MS1 or MS/MS scans. Instead, Hex-HNAc-HA-IPC and Hex-HN-HA-IPC were observed to be the dominant GIPC structure alongside other minor species including HN(Ac)-HA-IPC, $(Hex)_2$-HN(Ac)-HA-IPC and $(Hex)_3$-HN-HA-IPC, which is similar to rice root/leaves [25] and tobacco cultured cells [31]. Up to three hexose units were found to attach to the core

structure in barley roots, while in tobacco cultured cells up to additional five sugar units linked to the core structure including pentose units were discovered [33]. LCB composition of GIPC was similar to Cer species, comprising t18:0 and t18:1. Unlike previous experiments in the related cereal crop species rice [25], we were not able to find GIPCs containing dihydroxy LCBs in barley. We observed the LCBs in GIPCs to be preferentially acylated with VLCFA (≥ 22) with C24 as the predominant FA.

*3.2.4 Sterol derivatives*

In contrast to mammalian cells, which contain only one sterol subclass (cholesterol), barley can synthesize four subclasses of sterols including campesterol (ST_28:1), sitosterol (ST_29:1), stigmasterol (ST_29:2) and isofucosterol (ST_29:2) (Figure S1, Supplementary data). Fragmentation of ammonium adducts of SG and ASG induces neutral loss of all attached acyl and glucoside moieties on the respective sterol backbone producing a characteristic sterol anion. The characteristic sterol anion observed in MS/MS spectra, in conjunction with precursor ion match and RT behavior, is vital in SG and ASG identification (Table S1, Supplementary data).

The hydrophilic SGs were detected with early elution times (3 − 5 min). Among them, Glc-stigmasterol and Glc-isofucosterol are isomeric in both precursor ion and the characteristic sterol anion. Based on previous literature [34], separation of Glc-stigmasterol and Glc-isofucosterol can be achieved using reverse-phase chromatography. We predicted the precursor at *m/z* 592.458 and conducted an EICC at the MS1 level which showed two peaks eluting at 3.77 and 4.17 min, respectively. Further MS/MS spectra showed that fragmentation of compounds from the two peaks generated a major cation of *m/z* 395.368, which was the $[M-H_2O+H]^+$ of both the stigmasterol and isofucosterol backbone. The fragment ions below *m/z* 300 such as 295.227, 297.258 and 277.216 showed differences in abundance indicating the structural difference of the two compounds. However, we found it was impossible to assign the identity of Glc-stigmasterol and Glc-isofucosterol to either peak without the use of authentic standards. Therefore, we assigned the compound from the first peak as Glc-ST-1_ 29:2 (RT 3.77 min) and the following

compound as Glc-ST-2_29:2 (RT 4.17 min) (Figure S3, Supplementary data). A similar pair of isomers for ASG of stigmasterol/isofucosterol were also observed and named in a corresponding manner.

ASGs are more hydrophobic because of the FAs attached to the sterol backbone which show a later elution time in the system used in this study. Fatty acyl chains in ASGs were observed to be mainly C16:0, C18:2 and C18:3, followed by C18:1. FA chains with carbon number above 20 were hardly detected (Table S1, Supplementary data).

*3.3 Construction of sPRM assays for rapid targeted profiling*

As discussed previously, MS/MS data has several advantages over MS1 data including the ability to differentiate certain isomers of diacyl-GP/GLs, SPs and STs. Therefore, targeted profiling was carried out with MS/MS data acquired from sPRM assays. Using a RT scheduling window of 2 min and accumulation time of 25 ms, four sPRM assays made up of less than 18 mins running time in each assay were finally constructed to monitor the 634 identified lipid species. The first assay covers 291 species from PC/LysoPC, PE/LysoPE, PG/LysoPG, PS, MGDG/MGMG and DGDG/DGMG consisting of a total of 74 MS/MS experiments conducted in every 1.9 s duty cycle. The second assay covers 76 species from PI/LysoPI, SQDG/SQMG, GlcADG, and CL; the third assay covers 125 species from DAG, SG, ASG, Cer and HexCer; and the fourth assay covers all 142 GIPC species (Table S1, Supplementary data).

Compared to MRM assays, the high-resolution MS/MS spectra in PRM assays ensure more accurate precursor-product transition detection. For example, one of the major characteristic ions of MGDG in negative ion mode is *m/z* 253.0923, corresponding to galactosylglycerol of $[C_9H_{16}O_8]^-$. For MGDG species containing FA 16:1, a fatty acyl fragment of *m/z* 253.2168 is also generated. In MRM assays on QqQ or QTRAP instruments, the above two fragments will appear as a single peak due to the wide isolation window of the quadrupole (~0.7 Da); while in comparison, the two ions can be completely separated in high-resolution MS/MS by a TOF detector. Since fatty acyl fragments were employed to profile MGDG species, interference from the galactosylglycerol fragment can be avoided (Figure 4).

435 The acquisition rate is another major concern when performing large-scale lipid profiling based on
436 precursor-product transitions. The number of compounds that can be monitored in a PRM assay depends
437 largely on the MS/MS scan rate of the HRMS. Most previous PRM applications were achieved on Q-
438 Orbitrap, where a maximum 20 precursors can be multiplexed in a PRM assay [8, 35]. Contrastingly, the
439 6600 QqTOF is capable of a high MS/MS scan rate enabling multiplexing of up to 100 precursors without
440 sacrificing resolution on product ions, which currently provides the best HRMS for large scale profiling
441 using PRM [36]. Moreover, the wide polarity range of plant lipids usually results in a scattered RT
442 distribution in reverse-phase chromatography, which is an advantage to multiplex MS/MS experiments in
443 sPRM assays when using RT scheduling. Admittedly, compared with MRM on a QqQ or QTRAP which
444 can accommodate several hundreds of MS/MS experiments with a 1 − 5 ms dwell time\accumulation
445 time, the capacity of MS/MS experiments in PRM assays on a 6600 is still inferior [2]. One advantage of
446 PRM is that for a single compound, one MS/MS experiment can achieve accurate identification and
447 precise product ion selection from complete and high-resolution MS/MS spectra. While in MRM assays,
448 multiple MS/MS experiments are usually required to ensure proper peak-picking for profiling or
449 quantification.
450 It is important to note that each lipid species was profiled by relative peak area of one or multiple product
451 ions in our study instead of using absolute concentration. Absolute quantification of lipid species requires
452 calibration curves for each analyte. To eliminate possible matrix effects, calibration curves are acquired
453 via either spiking normal standards into analyte-free matrix or spiking isotope-labelled standard into real
454 samples. However, due to limited availability of commercial lipid standards, absolute quantification of
455 over 600 lipid species in LC-MS based lipidomics is impractical. Previous studies have also argued that
456 the main advantage of LC/MS based lipidomics lies in comparison across groups/treatments such as
457 plants under biotic and abiotic stress (i.e. salt, drought, cold) or after modification of certain genes (i.e.
458 silence, overexpression) rather than absolute quantification [3]. Comparison of fold changes are usually
459 the major focus in these studies and can be calculated directly from peak area/response.

460 sPRM assays in our experiment also offer a comparable linearity range (3 – 4 orders) and reproducibility
461 to traditional MRM assays on QqQ or QTRAP instruments [37, 38]. Linearity and reproducibility were
462 evaluated by exogenous lipid standards. Each exogenous lipid was comprised of a combination of FAs
463 that were known not to be present in the samples. Of the total 23 lipid classes measured, we were able to
464 obtain 13 lipid standards. No commercial standards were available for the other 10 classes (ASG, SG,
465 MGDG, MGMG, DGDG, DGMG, SQDG, SQMG, GlcADG and GIPC). To evaluate linearity of PRM
466 assays, barley extracts were spiked with a set of lipid standards. Six concentrations of each standard lipid
467 species in barley extract, spanning from 0.01 μM (10 nM) to 20 μM (20,000 nM), were measured in
468 triplicate in uPRM mode. The $r^2$ and dynamic range were calculated for both levels and summarized in
469 Table 3.
470 All lipid standards displayed excellent peak area linearity across the concentration range between 10 nM
471 and 20,000 nM in the injected sample with $r^2$ values above 0.9900 in MS/MS profiling. The specificity of
472 detection in MS/MS experiments was ensured by unique transitions and use of a narrow mass range
473 during product ion selection. Chromatography of product ions from MS/MS experiments usually
474 displayed very low or even no background signal, leading to a lower LOD and wider linear range. The
475 percent coefficient of variation (CV) of peak areas for each standard in each concentration was also
476 calculated for each concentration level. Most CVs were below 20% except at some of the lowest
477 concentrations, indicating good reproducibility (data not shown).
478
479 *3.4 Integrating targeted and untargeted profiling to a salt stress study in barley roots*
480 In our experiments, targeted lipid analysis was first performed on extracts from control and salt-treated
481 barley roots to unravel changes following exposure to salt stress. Four independent barley root lipid
482 extracts from each of the two groups (control and salt-treated) were analysed for the 634 lipid species
483 identified in untreated barley root extracts. As a result, 577 lipid species were well profiled with CV ≤
484 30% in PBQCs from both control and salt-treated root extracts (Table S2, Supplementary data). A
485 heatmap (Figure 5) using Euclidean distances and the Ward's algorithm was generated to provide an

overview of the difference between the control and salt-treated groups. Control and salt-treated samples were clustered with distinct variation of lipid levels in several classes. Most diacyl-GPs and GIPCs in the salt-treated group were present with higher abundance, while more lyso-species and diacyl-GLs (except DAG) were observed to be present in higher amounts in control samples.

To further investigate the significance of changes in individual species, compounds with an adjusted *p*-value below 0.05 in Student *t*-test and FC-value above 2 or below 0.5 as cut-off parameters were selected. These 221 compounds included 101 GPs, 63 GLs, 56 SPs and 1 ST. Within GP classes, most PIs (13 out of 15), PSs (24 out of 28) and PGs (17 out of 22) were among them, with more than 2 times higher abundance in the salt-treated group (Table S2, Supplementary data). Only 6 PEs (out of 43) and 7 PCs (out of 42) show a significant higher concentration which is surprising considering their relatively large number of different individual lipids. In GL classes, 55 of 56 species are from polar diacyl or mono-acyl classes. Only one DAG species was significantly affected by salt stress. Almost 90% of significantly altered SPs are GIPCs with 50 species changed upon salt stress. Most of the GIPC species showing higher levels in salt-treated samples (39 of 40) contained hydroxylated FAs on ceramide backbone. In the case of Hex-HNAc-HA-IPC series of GIPCs, all the species containing a hydroxylated FA show significant higher ($p < 0.01$) concentrations in salt-treated samples; while only one non-FA-hydroxylated species was observed with significant change (Figure 6a). This pattern of change suggests that plant responses to salt stress might induce FA-hydroxylation of GIPC. However, in the Hex-HN-HA-IPC series of GIPCs, such significant changes in lipids with hydroxylated FAs were not evident; instead, two non-FA-hydroxylated species exhibited decreased levels in salt-treated samples (Figure 6b). The FA-hydroxylation process presumably has a bias to GIPCs with a sugar head group containing HNAc.

The extended coverage on our platform incorporates GlcADGs and CLs, which were only recently profiled in plants [29, 39]. GlcADG is a novel GL class found to be accumulated when plants encounter phosphorus deficiency. GlcADG are believed to be mainly located in plastid/chloroplast membranes [29, 40]. We observed GlcADGs with a shorter FA chain 14:0 seems to accumulate upon salt stress (Figure 6c). Cardiolipin has rarely been mentioned in previous lipid studies on abiotic stress. We found that levels

512 in most CL species were shown to be significantly elevated under salt stress (Figure 6d). CLs are mainly
513 present in mitochondria and in *Arabidopsis* they have been shown to play a crucial role in maintaining
514 mitochondrial function under stress in studies of CARDIOLIPIN SYNTHASE gene *(cls1)* T-DNA
515 insertion mutants [41]. The various changes in the levels of plastidic lipids (PG, DGDG, GlcADG etc.)
516 and extra-plastidic lipids (CL, PC, PE, PS, PI, GIPCs etc.) suggests that salt-induced membrane
517 remodeling may occur differently for different organelle membranes [29, 42].
518 Apart from comparison of identified lipid species, direct comparison of mass features in MS1 data can
519 potentially generate unexpected insights (i.e. appearance of novel lipids under stress) which might be
520 missed in a targeted approach. Using the MarkerView software, 1281 unknown features in positive ion
521 mode and 1068 unknown features in negative ion mode were obtained with CVs ≤ 30% in PBQC samples
522 after excluding features belonging to the identified species. Initially to process untargeted data analysis,
523 principal component analysis (PCA) models on the combination of positive and negative features were
524 employed to provide an overview of the clustering of all extracted mass features. Groups of control and
525 salt-treated samples were clearly separated by PCA (Figure 7a) with the total variance of PC1 and PC2
526 greater than 90%, suggesting the existence of compounds which exhibited significantly different levels in
527 the two treatment groups in addition to the targeted lipid species.
528 To further investigate mass features that contribute to the difference, similar Student *t*-test with
529 Benjamini-Hochberg FDR correction and fold change analysis as in targeted lipidomics were employed
530 and displayed in a volcano plot (Figure 7b). In this way, 888 features including 479 features in positive
531 ion mode and 309 features in negative mode are shown with significant difference between the two
532 groups with adjusted *p*-values below 0.05 and FC values above 2 or below 0.5. Further annotation and
533 characterisation of these features is yet to be carried out.
534

## 4. Conclusion

In this study, comprehensive and accurate lipid discovery was achieved by combining strategies of building block restriction, high mass accuracy of MS1 data, RT behavior in reversed phase separation and MS/MS spectral analysis. Simultaneously, we constructed sPRM assays to achieve rapid profiling of compounds with high-resolution MS/MS data. In addition, MS1 data in PRM assays also enabled high-resolution (~ resolving power of 35,000) untargeted lipid profiling. Emerging targeted and untargeted lipidomics analysis on a single 6600 TripleTOF$^{TM}$ platform provides great economic benefits and experimental accessibility. The targeted methodology could also be used in a semi- and fully quantitative manner if appropriate standards are available and calibration curves are employed. In addition, the untargeted profiling data obtained can be directly compared between groups to search for potential biomarkers that, for example, could distinguish between disease states, stress-or toxicity-related changes and used to determine the most discriminant features. In conclusion, our novel method combines untargeted and targeted lipidomics methodologies into a single platform and provides avenues for a comprehensive investigation of lipidomic composition and alteration.

## 5. Acknowledgements

This project and U.R. were funded through an Australian Research Council (ARC) Future Fellowship program. D.Y has been funded through a Melbourne International Research Scholarship (MIRS) (University of Melbourne). I.F. was funded by the German Research Council (DFG, INST 186/1167-1). U.R., I.F. and D.Y. were also supported by a University Australia– Germany Joint Research Cooperation Scheme (DAAD 57140637). LC-MS experiments were carried out at Metabolomics Australia which is supported by funds from the Australian Government's National Collaborative Research Infrastructure Scheme (NCRIS) administered through Bioplatforms Australia (BPA) Ltd. The authors want to thank James A. Broadbent (SCIEX) for his assistance with 6600 TripleTOF™ operation and PRM assays setup. We also want to thank Dr. Stuart Roy (University of Adelaide) for providing barley seeds; and Mrs. Nirupama Jayasinghe, Mrs. Himasha Mendis and Ms. Veronica Lui (Metabolomics Australia) for GC-MS FAME analysis and quantification.

**Table 1. Chromatographic and mass spectrometry conditions for different lipid classes in sPRM assays including gradient, ion polarity, precursor ion type and collision energy (CE).**

| Category | Class | Gradient | Ionization mode | Precursor ion type | CE (V) |
|---|---|---|---|---|---|
| Glycerol-phospholipid (GP) | LysoPC | G1 | Neg | $[M+OAc]^-$ | −45 |
| | LysoPE | G1 | Neg | $[M-H]^-$ | −45 |
| | LysoPG | G1 | Neg | $[M-H]^-$ | −45 |
| | LysoPI | G1 | Neg | $[M-H]^-$ | −65 |
| | PC | G1 | Neg | $[M+OAc]^-$ | −45 |
| | PE | G1 | Neg | $[M-H]^-$ | −45 |
| | PG | G1 | Neg | $[M-H]^-$ | −45 |
| | PI | G1 | Neg | $[M-H]^-$ | −65 |
| | PS | G1 | Neg | $[M-H]^-$ | −45 |
| | CL | G1 | Neg | $[M-H]^-$ | −65 |
| Glycerolipid (GL) | MGMG | G1 | Neg | $[M+OAc]^-$ | −45 |
| | DGMG | G1 | Neg | $[M+OAc]^-$ | −45 |
| | SQMG | G1 | Neg | $[M-H]^-$ | −65 |
| | MGDG | G1 | Neg | $[M+OAc]^-$ | −45 |
| | DGDG | G1 | Neg | $[M+OAc]^-$ | −45 |
| | SQDG | G1 | Neg | $[M-H]^-$ | −65 |
| | GlcADG | G1 | Neg | $[M-H]^-$ | −65 |
| | DAG | G2 | Pos | $[M+NH_4]^+$ | +40 |
| Sterol Lipid (ST) | ASG | G2 | Pos | $[M+NH_4]^+$ | +40 |
| | SG | G2 | Pos | $[M+NH_4]^+$ | +40 |
| Sphingolipid (SP) | Cer | G2 | Pos | $[M+H]^+$ | +40 |
| | HexCer | G2 | Pos | $[M+H]^+$ | +40 |
| | GIPC | G3 | Pos | $[M+H]^+$ | +65±10 |

Abbreviations: PC: phosphatidylcholine; PE: phosphatidylethanolamine; PG: phosphatidylglycerol; PI: phosphatidylinositol; PS: phosphatidylserine; CL: cardiolipin; MGDG: monogalactosyl diacylglycerol; MGMG: monogalactosyl monoacylglycerol; DGDG: digalactosyl diacylglycerol; DGMG: digalactosyl monoacylglycerol; SQDG: sulfoquinovosyl diacylglycerol; SQMG: sulfoquinovosyl monoacylglycerol; GlcADG: glucuronosyl diacylglycerol; DAG: diacylglycerol; SG: sterol glycoside; ASG: acylated sterol glucoside; Cer: ceramide; HexCer: monohexosyl ceramide; GIPC: glycosyl inositol phosphorylceramide; Pos: positive ion mode; Neg: negative ion mode; OAc: acetate; G1/2/3: Gradient 1/2/3.

Column A: Agilent Poroshell EC-C18 (100 mm × 2.1 mm, 2.7 μm); Column B: Agilent ZORBAX Eclipse XDB C18 (100 mm × 2.1 mm, 1.8 μm).

577 **Table 2: Summary of lipid classes identified in barley root extracts shown as number of detected**
578 **IDs. Species were detected at the level of FA/LCB/sterol composition.**

| Category | Class | Number of IDs |
|---|---|---|
| GP | PC/LysoPC | 42/17 |
| (n = 209) | PE/LysoPE | 43/17 |
| | PG/LysoPG | 22/7 |
| | PI/LysoPI | 15/5 |
| | PS | 29 |
| | CL | 12 |
| GL | MGDG/MGMG | 43/16 |
| (n = 190) | DGDG/DGMG | 38/17 |
| | SQDG/SQMG | 20/7 |
| | GlcADG | 17 |
| | DAG | 32 |
| SP | HexCer | 47 |
| (n = 215) | Cer | 26 |
| | GIPC | 142 |
| ST | SG | 4 |
| (n = 20) | ASG | 16 |
| Total | | 634 |

579

580 Abbreviations: ASG: acylated sterol glucoside; Cer: ceramide; CL: cardiolipin; DAG: diacylglycerol;
581 DGDG: digalactosyl diacylglycerol; DGMG: digalactosyl monoacylglycerol; FA: fatty acid; GL:
582 glycerolipid; GlcADG: glucuronosyl diacylglycerol; GP: glycerolphospholipid; HexCer: monohexosyl
583 ceramide; LCB: long chain base; MGDG: monogalactosyl diacylglycerol; MGMG: monogalactosyl
584 monoacylglycerol; PC: phosphatidylcholine; PE: phosphatidylethanolamine; PG: phosphatidylglycerol;
585 PI: phosphatidylinositol; PS: phosphatidylserine; SG: sterol glycoside; SP: sphingolipid; SQDG:
586 sulfoquinovosyl diacylglycerol; SQMG: sulfoquinovosyl monoacylglycerol; ST: sterol derivative.
587

588 **Table 3: Evaluation of linearity ($r^2$) and dynamic range in the PRM assay of standards in the**
589 **presence of barley root extract.**

| Lipid standard | $r^2$ | Dynamic range (nM) |
|---|---|---|
| PC(13:0/13:0) | 0.9958 | 10-20,000 |
| PE(12:0/12:0) | 0.9950 | 10-20,000 |
| PG(12:0/12:0) | 0.9970 | 10-20,000 |
| PS(12:0/12:0) | 0.9980 | 10-20,000 |
| PI(18:0/20:4) | 0.9955 | 10-20,000 |
| LysoPC(13:0) | 0.9952 | 10-20,000 |
| LysoPE(13:0) | 0.9944 | 10-20,000 |
| LysoPG(13:0) | 0.9932 | 10-20,000 |
| LysoPI(13:0) | 0.9953 | 10-20,000 |
| CL(T14:0) | 0.9913 | 10-20,000 |
| Cer(d18:1/12:0) | 0.9996 | 10-20,000 |
| GlcCer(d18:1/12:0) | 0.9977 | 10-20,000 |
| DAG(18:0/20:4) | 0.9907 | 10-20,000 |

590

591 Abbreviations: Cer: ceramide; CL: cardiolipin; DAG: diacylglycerol; GlcCer: monoglucosyl ceramide;
592 PC: phosphatidylcholine; PE: phosphatidylethanolamine; PG: phosphatidylglycerol; PI:
593 phosphatidylinositol; PS: phosphatidylserine.

594

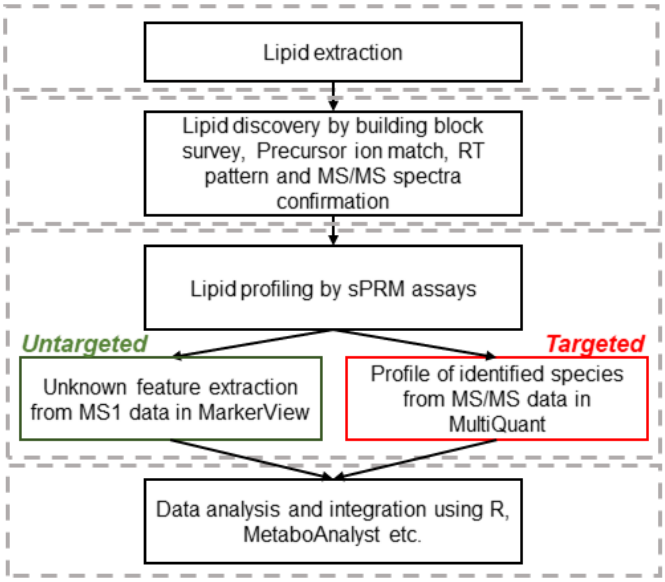


595

596 **Figure 1: Workflow of lipid discovery and profiling by HPLC-ESI-QqTOF.**

597 Abbreviations: sPRM: scheduled parallel reaction monitoring; RT: retention time

598

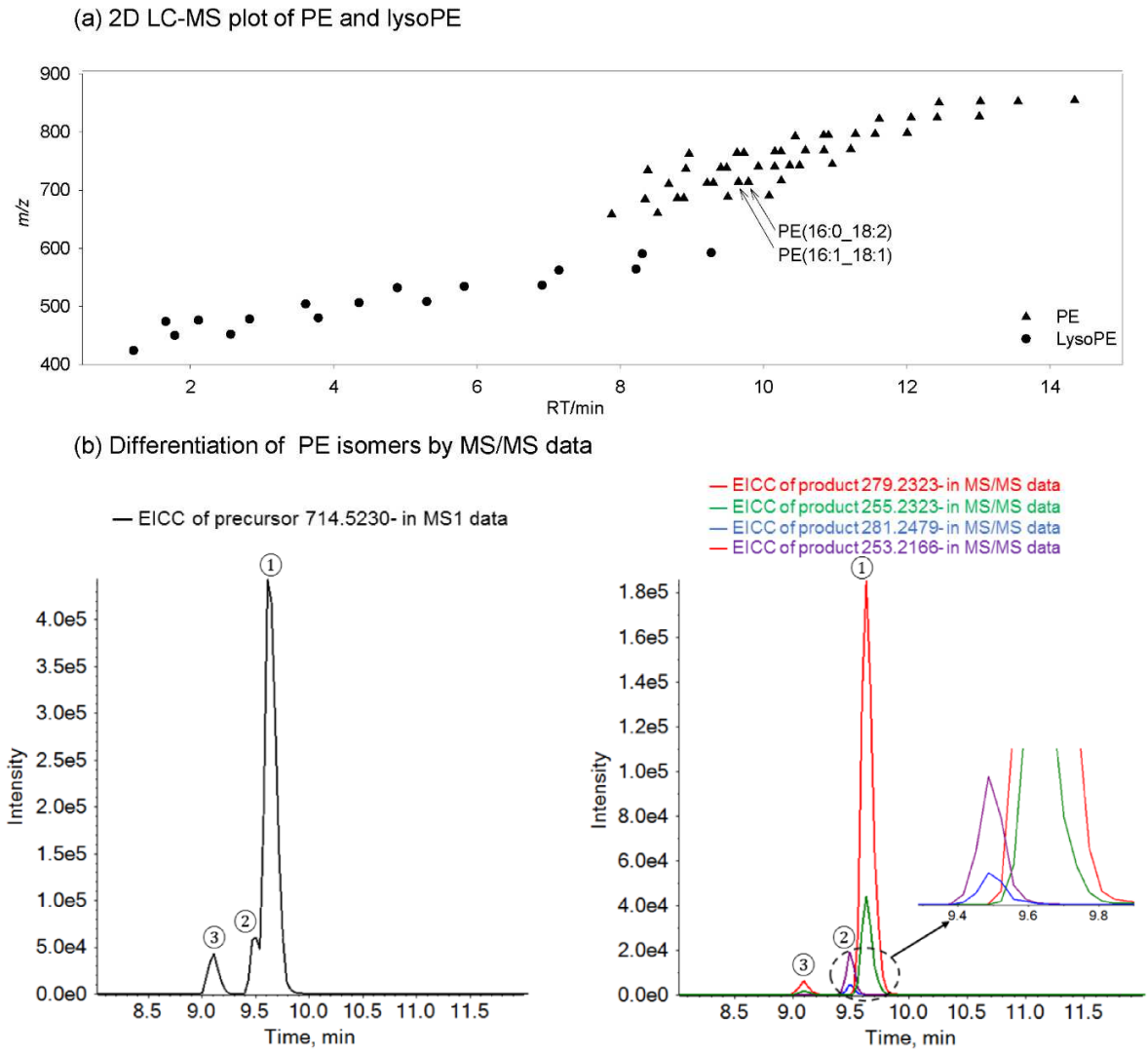


**Figure 2: 2D LC-MS plot of PE and lysoPE species (a) and differentiation of isomers using MS/MS data (b).**

(a) PEs: triangles; LysoPEs: circles. (b) PE(16:0_18:2) and PE(16:1_18:1) have the exact same molecular weight as $[M-H]^-$ *m/z* 714.5230 but differ in fatty acyl distribution in the *sn*-1/2 position. EICC of the precursor *m/z* 738.507 in MS1 scan exhibited two slightly separated peaks from 9.4 min to 10.0 min (left figure). The two peaks are well deconvoluted and interpreted using MS/MS data (right figure). EICC of the four carboxylate anions in MS/MS spectra shows that peak ① corresponded to PE(16:0_18:2); while peak ② corresponded to PE(16:1_18:1). This graph also shows baseline chromatographic separation between PE(34:3) (peak ③) and PE(34:2), avoiding any isotopic interference arising from FA fragments. EICC: extracted ion count chromatogram .

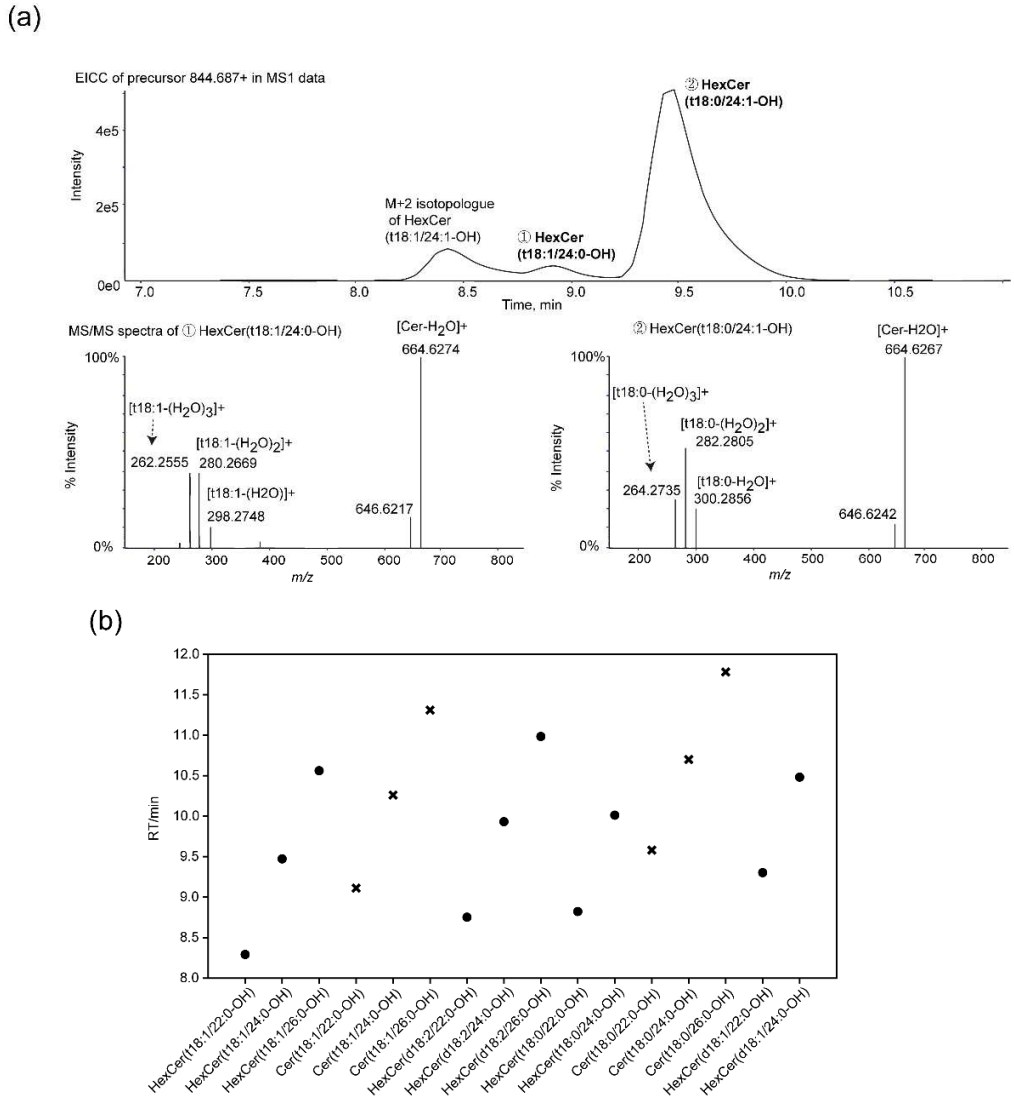


**Figure 3: Differentiation of isobaric and isomeric ceramide-containing sphingolipid species in barley root extracts by MS/MS spectra (a) and RT pattern (min) (b).**

(a) MS/MS spectra of ① HexCer(t18:0/24:1-OH) (RT 8.91 min) and ② HexCer(t18:1/24:0-OH) (RT 9.47 min). They have a similar charged ceramide fragment (*m/z* 664.627+) and its dehydrates but differ in the cluster of fragments from charged LCBs. (b) For sphingolipid species containing the same fatty acid chain, RT values according to LCBs were t18:1 < d18:2 < t18:0 < d18:1. Cer species eluted 0.8 – 1 min later than its corresponding HexCer species. HexCer species: black circles; Cer species: X crosses. RT: retention time; Cer: ceramide; HexCer: hexosyl ceramide; LCB: long chain base.

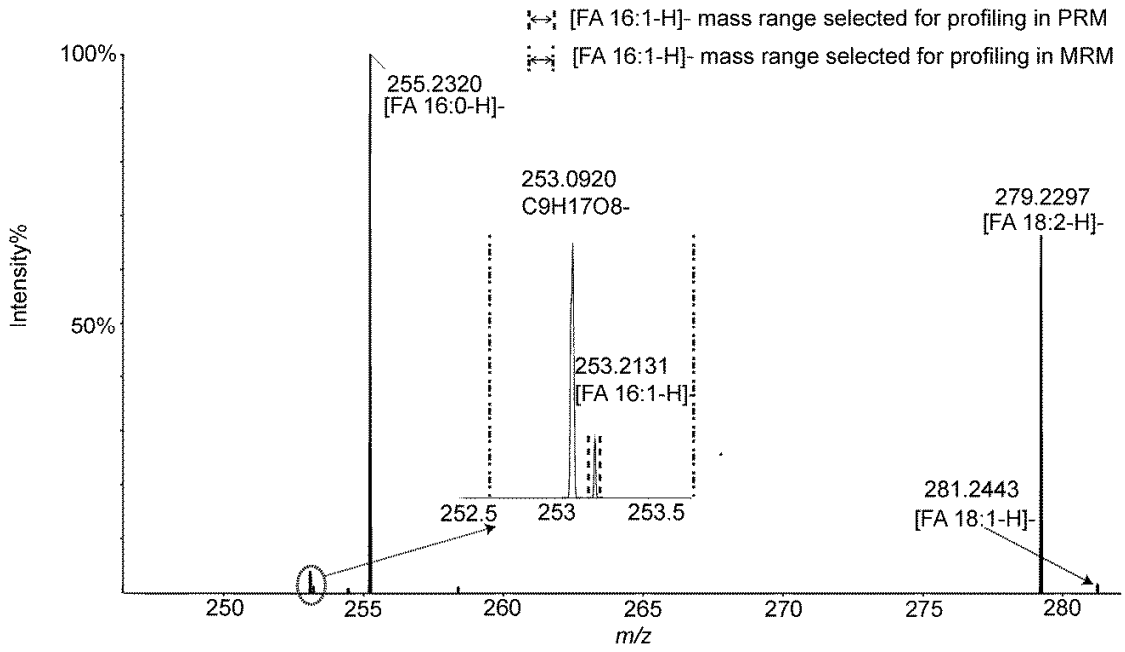


**Figure 4: The high-resolution MS/MS spectra in PRM assays ensure more accurate precursor-product transition selection than in MRM assays when profiling MGDG(16:1_18:1).**

MGDG(16:1_18:1) and MGDG(16:0_18:2) were not well resolved chromatographically. The *m/z* 253.0920 ion corresponding to galactosylglycerol of $[C_9H_{16}O_8]^-$ resulted from both species. *m/z* 253.2131 was picked as product ion only for profiling. MGDG(16:1_18:1) was not interfered with by *m/z* 253.0920 due to high-resolution MS/MS spectra and a 100 ppm peak-picking width in PRM assays; while in traditional MRM assays, the two ions could not be detected separately with a 0.7 Da isolation window.

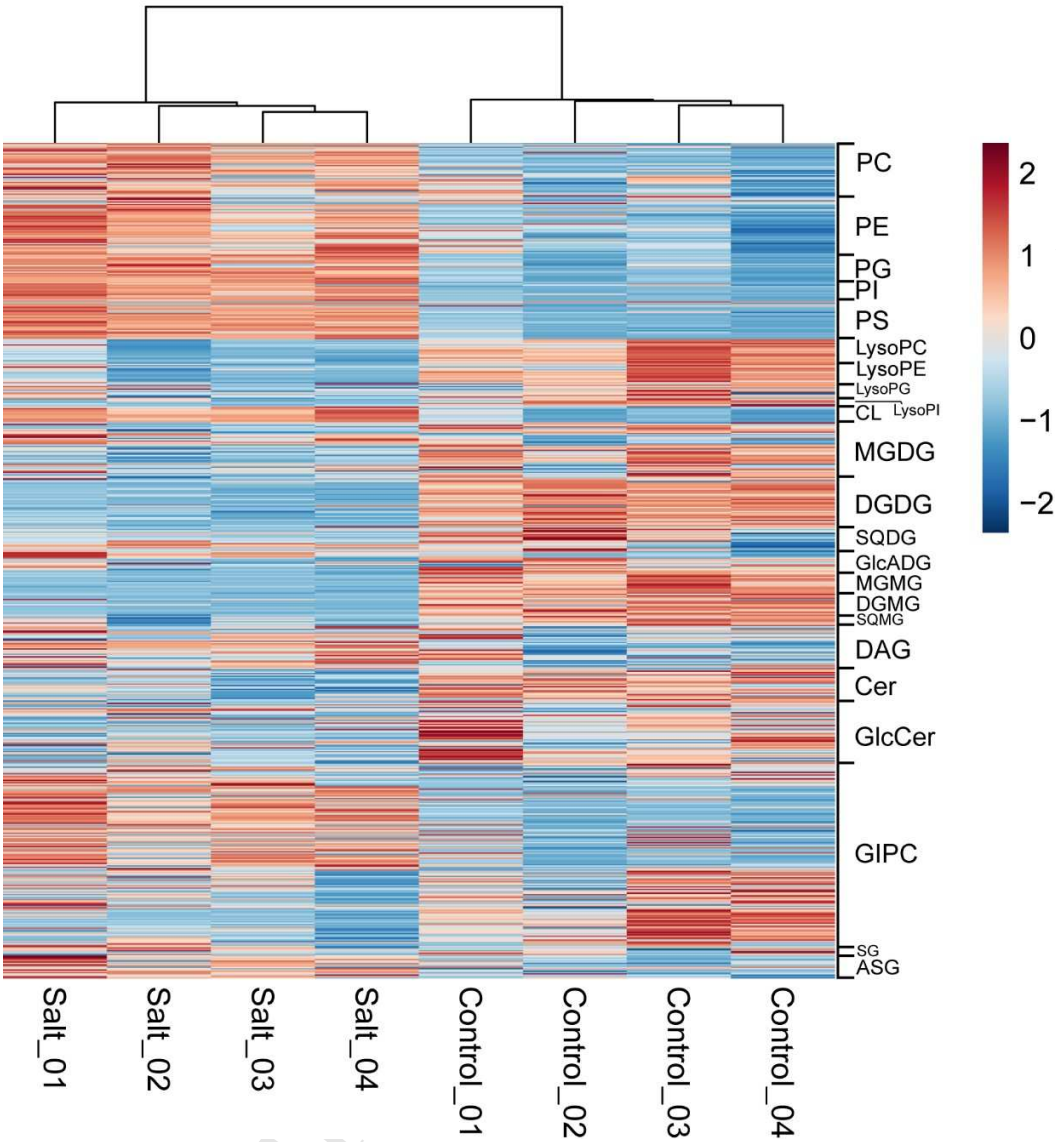


**Figure 5: Heatmap visualization and hierarchical clustering analysis on targeted lipid levels in control and salt-treated barley root extracts using Euclidean distances and the Ward's algorithm.** Clustering of control and salt-treated samples is described by the dendrogram on the top. Rows: lipid species; Columns: samples; Color key indicates fold change of peak area in control relative to salt. ASG: acylated sterol glucoside; Cer: ceramide; CL: cardiolipin; DAG: diacylglycerol; DGDG: digalactosyl diacylglycerol; DGMG: digalactosyl monoacylglycerol; FA: fatty acid; GIPC: glucosyl inositol phosphorylceramide; GL: glycerolipid; GlcADG: glucuronosyl diacylglycerol; GP: glycerolphospholipid; HexCer: monohexosyl ceramide; LCB: long chain base; MGDG: monogalactosyl diacylglycerol; MGMG: monogalactosyl monoacylglycerol; PC: phosphatidylcholine; PE: phosphatidylethanolamine; PG: phosphatidylglycerol; PI: phosphatidylinositol; PS: phosphatidylserine; SG: sterol glycoside; SP:

639 sphingolipid; SQDG: sulfoquinovosyl diacylglycerol; SQMG: sulfoquinovosyl monoacylglycerol; ST:
640 sterol derivative.
641

642

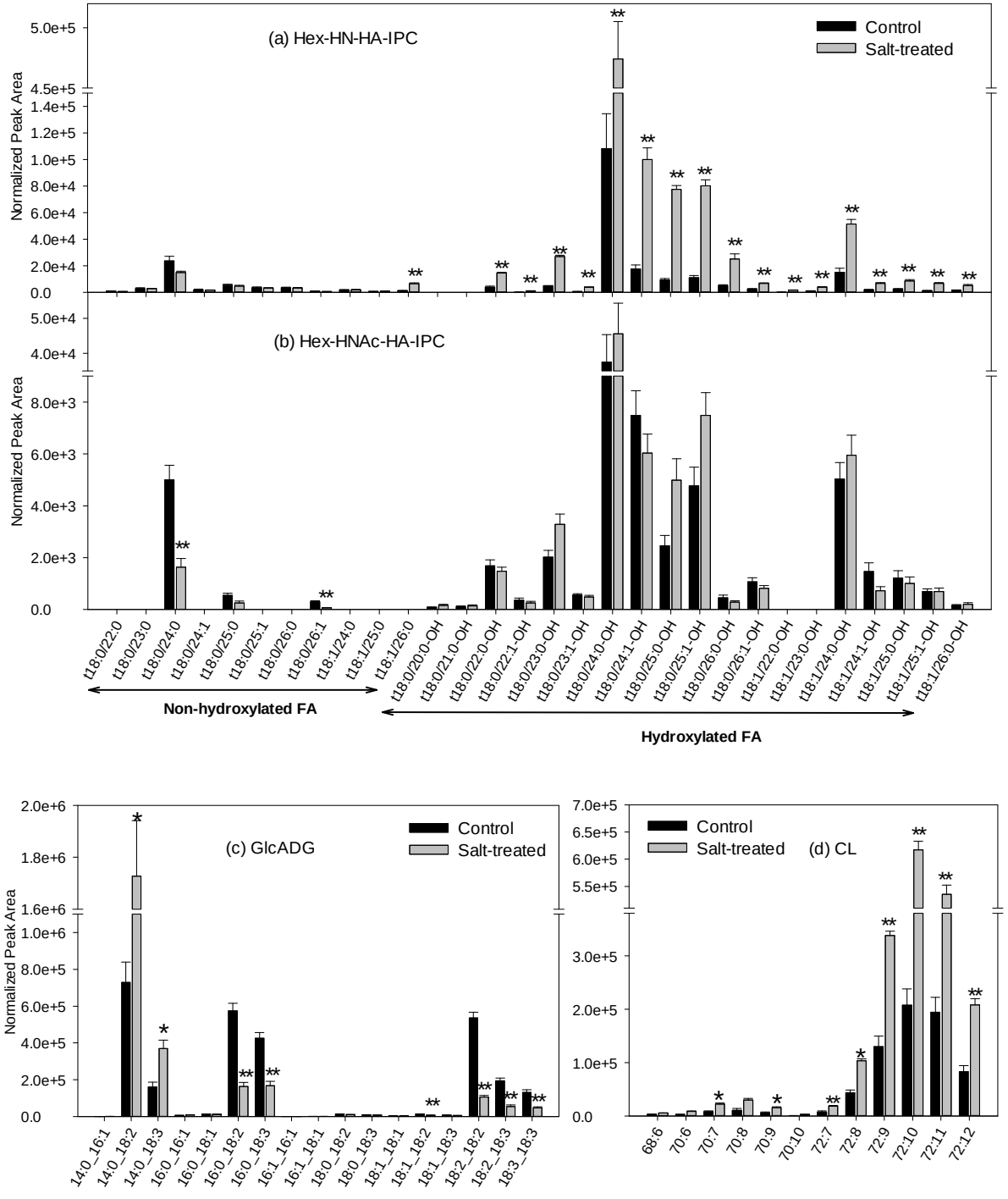


643

644 **Figure 6: Profile of Hex-HN-HA-IPC (a) and Hex-HNAc-HA-IPC (b) series of GIPCs, GlcADG (c)**
645 **and CL (d) in control and salt-treated barley root extracts (n = 4) expressed as normalized peak**
646 **area.**

647 Black bars correspond to control group; grey bars correspond to salt-treated group. Peak area is
648 normalised to the value equivalent to 250 mg fresh barley weight. Significance was evaluated by the
649 Student's *t*-test followed by Benjamini-Hochberg false discovery rate (FDR) correction; $*p < 0.05$; $**p <$
650 0.01; mean + SE. CL: cardiolipin; GlcADG: glucuronosyl diacylglycerol; Hex: hexosyl; HN: N-
651 Acetylhexosamine; HNAc: hexosamine; HA: hexuronic acid; IPC: inositol phosphorylceramide.
652

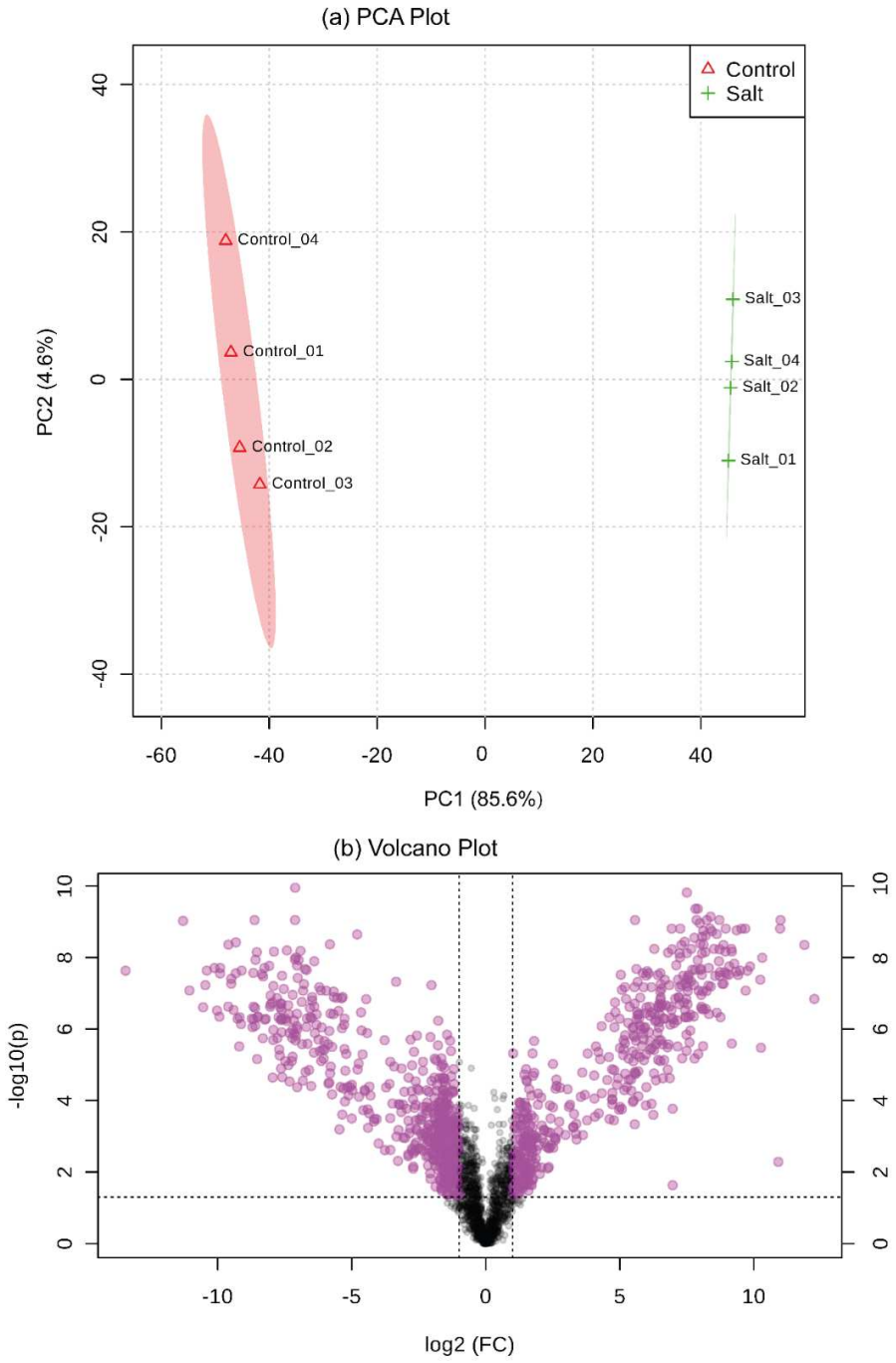


**Figure 7: Principal Component Analysis (PCA) (a), and Volcano plot (b) for 2349 unidentified features together from positive and negative ion modes in control and salt-treated barley root extracts.**

(a) Two-dimensional scatter plot of PCA displaying Components 1 and 2, which account for 85.6% and 4.6%, respectively. Control and salt-treated samples are clearly separated by PCA. Control: red triangle;

659 salt-treated: green X cross. (b) A volcano plot was performed to determine responsive difference for
660 individual lipids between two groups. Each circle represents a lipid. Lipids with an adjusted *p* value
661 below 0.05 and fold-change value above 2 or below 0.5 are represented as purple circles.
662

## References

[1] S.M. Lam, G. Shui, Lipidomics as a Principal Tool for Advancing Biomedical Research, J. Genet. Genomics, 40 (2013) 375-390.

[2] T. Cajka, O. Fiehn, Toward Merging Untargeted and Targeted Methods in Mass Spectrometry-Based Metabolomics and Lipidomics, Anal. Chem., 88 (2016) 524-545.

[3] P. Tarazona, K. Feussner, I. Feussner, An enhanced plant lipidomics method based on multiplexed liquid chromatography-mass spectrometry reveals additional insights into cold- and drought-induced membrane remodeling, The Plant J, 84 (2015) 621-633.

[4] R.P. Haslam, I. Feussner, Green light for lipid fingerprinting, Biochim. Biophys. Acta, 1862 (2017) 782-785.

[5] B. Schilling, B. MacLean, J.M. Held, A.K. Sahu, M.J. Rardin, D.J. Sorensen, T. Peters, A.J. Wolfe, C.L. Hunter, M.J. MacCoss, Multiplexed, scheduled, high-resolution parallel reaction monitoring on a full scan QqTOF instrument with integrated data-dependent and targeted mass spectrometric workflows, Anal. Chem., 87 (2015) 10222-10229.

[6] J. Zhou, Y. Yin, Strategies for large-scale targeted metabolomics quantification by liquid chromatography-mass spectrometry, Analyst, 141 (2016) 6362-6373.

[7] A.C. Peterson, J.D. Russell, D.J. Bailey, M.S. Westphall, J.J. Coon, Parallel reaction monitoring for high resolution and high mass accuracy quantitative, targeted proteomics, Mol. Cell. Proteomics, 11 (2012) 1475-1488.

[8] J. Zhou, H. Liu, Y. Liu, J. Liu, X. Zhao, Y. Yin, Development and Evaluation of a Parallel Reaction Monitoring Strategy for Large-Scale Targeted Metabolomics Quantification, Anal. Chem., 88 (2016) 4478-4486.

[9] Z. Li, Y. Li, W. Chen, Q. Cao, Y. Guo, N. Wan, X. Jiang, Y.J. Tang, Q. Wang, W. Shui, Integrating MS1 and MS2 Scans in High-Resolution Parallel Reaction Monitoring Assays for Targeted Metabolite Quantification and Dynamic 13C-Labeling Metabolism Analysis, Anal. Chem., 89 (2017) 877-885.

[10] J. Zhou, C. Liu, D. Si, B. Jia, L. Zhong, Y. Yin, Workflow development for targeted lipidomic quantification using parallel reaction monitoring on a quadrupole-time of flight mass spectrometry, Anal. Chim. Acta, 972 (2017) 62-72.

[11] A. Triebl, J. Hartler, M. Trötzmüller, H.C. Köfeler, Lipidomics: Prospects from a technological perspective, Biochim. Biophys. Acta-Mol. Cell Biol. Lipids, 1862 (2017) 740-746.

[12] G.L. Andrews, B.L. Simons, J.B. Young, A.M. Hawkridge, D.C. Muddiman, Performance characteristics of a new hybrid triple quadrupole time-of-flight tandem mass spectrometer, Anal. Chem., 83 (2011) 5442.

[13] H. Tang, H. Fang, E. Yin, A.R. Brasier, L.C. Sowers, K. Zhang, Multiplexed Parallel Reaction Monitoring Targeting Histone Modifications on the QExactive Mass Spectrometer, Anal. Chem., 86 (2014) 5526-5534.

[14] J. Wu, D.M. Seliskar, J.L. Gallagher, The response of plasma membrane lipid composition in callus of the halophyte Spartina patens (Poaceae) to salinity stress, Am. J. Bot., 92 (2005) 852-858.

[15] R.G. Upchurch, Fatty acid unsaturation, mobilization, and regulation in the response of plants to stress, Biotechnol. Lett., 30 (2008) 967-977.

[16] W. van Leeuwen, L. Ökrész, L. Bögre, T. Munnik, Learning the lipid language of plant signalling, Trends Plant Sci., 9 (2004) 378-384.

[17] R. Munns, M. Tester, Mechanisms of salinity tolerance, Annu. Rev. Plant Biol., 59 (2008) 651-681.

[18] S.H. Natera, C.B. Hill, T.W. Rupasinghe, U. Roessner, Salt-stress induced alterations in the root lipidome of two barley genotypes with contrasting responses to salinity, Funct. Plant Biol., 43 (2016) 207-219.

[19] E. Fahy, S. Subramaniam, H.A. Brown, C.K. Glass, A.H. Merrill, R.C. Murphy, C.R.H. Raetz, D.W. Russell, Y. Seyama, W. Shaw, T. Shimizu, F. Spener, G. van Meer, M.S. VanNieuwenhze, S.H. White, J.L. Witztum, E.A. Dennis, A comprehensive classification system for lipids, J. Lipid Res., 46 (2005) 839-862.

[20] G. Liebisch, J.A. Vizcaíno, H. Köfeler, M. Trötzmüller, W.J. Griffiths, G. Schmitz, F. Spener, M.J. Wakelam, Shorthand notation for lipid structures derived from mass spectrometry, J. Lipid Res., 54 (2013) 1523-1530.

[21] D. Cao, A. Lutz, C.B. Hill, D.L. Callahan, U. Roessner, A quantitative profiling method of phytohormones and other metabolites applied to barley roots subjected to salinity stress, Front. Plant Sci., 7 (2017) 2070.

[22] K. Grillitsch, P. Tarazona, L. Klug, T. Wriessnegger, G. Zellnig, E. Leitner, I. Feussner, G. Daum, Isolation and characterization of the plasma membrane from the yeast Pichia pastoris, Biochim. Biophys. Acta-Biomembr., 1838 (2014) 1889-1897.

[23] C.B. Hill, A. Bacic, U. Roessner, LC-MS profiling to link metabolic and phenotypic diversity in plant mapping populations, Mass Spectrometry in Metabolomics: Methods and Protocols, Springer, New York, 2014.

[24] D. Riewe, J. Wiebach, T. Altmann, Structure annotation and quantification of wheat seed oxidized lipids by high resolution LC-MS/MS, Plant Physiol., 175 (2017) 600-618.

[25] T. Ishikawa, Y. Ito, M. Kawai‐Yamada, Molecular characterization and targeted quantitative profiling of the sphingolipidome in rice, The Plant J., 88 (2016) 681-693.

729 [26] W.W. Christie, X. Han, Characterization of lipids by electrospray ionization mass spectrometry,
730 Lipid Analysis, Fourth edition, Woodhead Publishing, 2012.
731 [27] V. Wewer, I. Dombrink, K. vom Dorp, P. Dörmann, Quantification of sterol lipids in plants by
732 quadrupole time-of-flight mass spectrometry, J. Lipid Res., 52 (2011) 1039-1054.
733 [28] T. Kind, K.-H. Liu, D.Y. Lee, B. DeFelice, J.K. Meissen, O. Fiehn, LipidBlast in silico tandem mass
734 spectrometry database for lipid identification, Nat. Methods, 10 (2013) 755-758.
735 [29] Y. Okazaki, H. Otsuki, T. Narisawa, M. Kobayashi, S. Sawai, Y. Kamide, M. Kusano, T. Aoki, M.Y.
736 Hirai, K. Saito, A new class of plant lipid is essential for protection against phosphorus depletion, Nat.
737 commun., 4 (2013) 1510.
738 [30] R. t'Kindt, L. Jorge, E. Dumont, P. Couturon, F. David, P. Sandra, K. Sandra, Profiling and
739 characterizing skin ceramides using reversed-phase liquid chromatography–quadrupole time-of-flight
740 mass spectrometry, Anal. Chem., 84 (2011) 403-411.
741 [31] C. Buré, J.-L. Cacas, S. Mongrand, J.-M. Schmitter, Characterization of glycosyl inositol phosphoryl
742 ceramides from plants and fungi by mass spectrometry, Anal. Bioanal. Chem., 406 (2014) 995-1010.
743 [32] J.-L. Cacas, C. Buré, F. Furt, J.-P. Maalouf, A. Badoc, S. Cluzet, J.-M. Schmitter, E. Antajan, S.
744 Mongrand, Biochemical survey of the polar head of plant glycosylinositolphosphoceramides unravels
745 broad diversity, Phytochemistry, 96 (2013) 191-200.
746 [33] C. Buré, J.L. Cacas, F. Wang, K. Gaudin, F. Domergue, S. Mongrand, J.M. Schmitter, Fast screening
747 of highly glycosylated plant sphingolipids by tandem mass spectrometry, Rapid Commun. Mass
748 Spectrom., 25 (2011) 3131-3145.
749 [34] R. Rozenberg, Phytosterol analysis and characterisation in spelt (Triticum aestivum ssp, spelta L.)
750 and wheat (T. aestivum L.) lipids by LC/APCI-MS. J. Cereal Sci., 38 (2003) 197.
751 [35] B. Peng, S.T. Weintraub, C. Coman, S. Ponnaiyan, R. Sharma, B. Tews, D. Winter, R. Ahrends, A
752 Comprehensive High-Resolution Targeted Workflow for the Deep Profiling of Sphingolipids, Anal.
753 Chem., 89 (2017) 12480-12487.
754 [36] F. Fenaille, P.B. Saint-Hilaire, K. Rousseau, C. Junot, Data acquisition workflows in liquid
755 chromatography coupled to high resolution mass spectrometry-based metabolomics: Where do we stand?,
756 J. Chromatogr. A, 1526 (2017) 1-12.
757 [37] K.M. MacDougall, J. McNichol, P.J. McGinn, S.J.B. O'Leary, J.E. Melanson, Triacylglycerol
758 profiling of microalgae strains for biofuel feedstock by liquid chromatography–high-resolution mass
759 spectrometry, Anal. Bioanal. Chem., 401 (2011) 2609-2616.
760 [38] M. Scherer, K. Leuthaeuser-Jaschinski, J. Ecker, G. Schmitz, G. Liebisch, A rapid and quantitative
761 LC-MS/MS method to profile sphingolipids, J. Lipid Res., 51 (7): 2001–2011.

762 [39] Y. Zhou, H. Peisker, P. Dörmann, Molecular species composition of plant cardiolipin determined by
763 liquid chromatography mass spectrometry, J. Lipid Res., 57 (2016) 1308-1321.
764 [40] P. Dörmann, “Galactolipids in plant membranes” in Encyclopaedia of Life Sciences, John Wiley &
765 Sons Ltd, Chichester. 2001.
766 [41] T. Romantsov, Z. Guan, J.M. Wood, Cardiolipin and the osmotic stress responses of bacteria,
767 Biochim. Biophys. Acta, 1788 (2009) 2092-2100.
768 [42] Y. Okazaki, K. Saito, Roles of lipids as signaling molecules and mitigators during stress response in
769 plants, Plant J., 79 (2014) 584-596.
770

- A lipidomics workflow merging targeted and untargeted approaches using PRM strategy
- Discovery of 2349 unknown features and 634 known lipid species in barley roots
- Rapid profiling of 291 species based on MS/MS data by a single injection using sPRM
- An application of the workflow on salt stress-induced lipid changes in barley roots